Numerical Methods in Civil Engineering, 7-2 (2022) 42-49

Numerical Methods in Civil Engineering

Journal Homepage: https://nmce.kntu.ac.ir/

Displacement Pattern in a Functionally Graded Transversely Isotropic, Half-Space Due to Dislocation

Maziar Kalantari[*] and Naser Khaji[**]

ARTICLE INFO

RESEARCH PAPER

Article history:
Received:
April 2022.
Revised:
June 2022.
Accepted:
June 2022.

Keywords:
Dislocation theory,
Transversely isotropic,
Finite fault,
Non-homogeneous materials

Abstract:

The forward solution of dislocation on the fault plane is one of the most important issues for earthquake source slip inversion. The dislocation on the fault plane, explained by the Burgers vector which is called slip, plays a fundamental role in estimating displacement patterns in the whole medium. In addition, obtaining displacement values in any point of a medium is possible by using the slip function on the fault plane and Green's function as medium properties. This study shows that various assumptions for earth materials result in significant differences in displacements. Therefore, due to the realistic ground motion simulations caused by future earthquakes, considering the properties of earth materials requires more attention. By implementing the elastostatic Green's functions and based upon line integral representations due to an arbitrary Volterra dislocation loop, elastic displacements and strains due to finite fault dislocations in a functionally graded transversely isotropic (FGTI) half-space material is presented. Also, numerical examples are provided to demonstrate the effect of material anisotropy on the internal and surface responses of the half-space.

1. Introduction

Forward solutions for dislocations of faults provide a useful means of finding the behavior of faults. Also, this phenomenon, by considering realistic materials as exist in nature, extensively clarifies many physical aspects of the underlying problem through a deeper understanding of the mathematical nature of the associated problem.

Displacement in solids induced by external load or dislocation is a topic of considerable interest in mechanics and has long been the subject of numerous studies for decades. Traditionally, the media are often assumed to be isotropic and homogeneous (e.g., [1-8] and references therein).

In recent decades, the increasing use of composite materials in modern technologies and engineering applications has become an incentive for extensive research, both basic and applied, into various failure modes of such materials.

Transversely isotropic (TI) model is able to appropriately represent the anisotropic behavior of most materials in various practical applications, such as composites, smart and intelligent materials, piezoelectrics, piezomagnetics [9-10], and many natural soils deposited through a geologic process of sedimentation over a period of time, where determining their displacements and stresses needs the anisotropy to be taken into account [11-16]. Therefore, the primary task is to choose a proper constitutive law of the medium. Thus, adding functionally graded materials (FGMs) as a rational assumption for continuous alteration of material properties with TI media can make a realistic medium that is very close to the nature of the soil. Therefore, a complex analysis associated with continuum modeling of soil can lead to an efficient and accurate result.

Most of the above-mentioned studies assumed soils are isotropic, TI, or anisotropic, since actual soils are seldom homogeneous and their properties usually vary with depth due to the effects of deposition, overburden, and confining pressure. Therefore, constant depth-profile properties for soil deposits may be a rather poor approximation to the real conditions and more advanced models are essential [17-19]. Many researchers considered the problem of the elastic

* *Ph.D., Faculty of Civil and Environmental Engineering, Tarbiat Modares University, P. O. Box 14115-397, Tehran, Iran.*

E-mail: maziar.kalantari@modares.ac.ir

** *Corresponding author: Ph.D., Civil and Environmental Engineering Program, Graduate School of Advanced Science and Engineering, Hiroshima University, Higashi-Hiroshima, 739-8527, Japan. E-mail: nkhaji@hiroshima-u.ac.jp*

response of inhomogeneous isotropic solids under different loading conditions for different patterns of material properties, such as linear, quadratic, power-law [20], and exponential functions [21-24]. Because of the practical simplification of the mathematical formulation, exponential variation for the FGMs is extensively used in the engineering literature [21, 25].

For the case of exponentially graded material, elastostatic and elastodynamic Green's functions of an exponentially graded transversely isotropic half-space were presented by [26] and [27], respectively. Kalantari and others have conducted comprehensive studies on the functionally graded transversely isotropic (FGTI) material for various kinds of loads [28-30, 40]. They showed the impact of materials' non-homogeneity on the response of various applied loads. Using our previous studies and based upon line integral representations due to an arbitrary Volterra dislocation loop [12,31], elastic displacements due to finite fault in an FGTI half-space are presented.

2. Statement of the Problem and Governing Equations

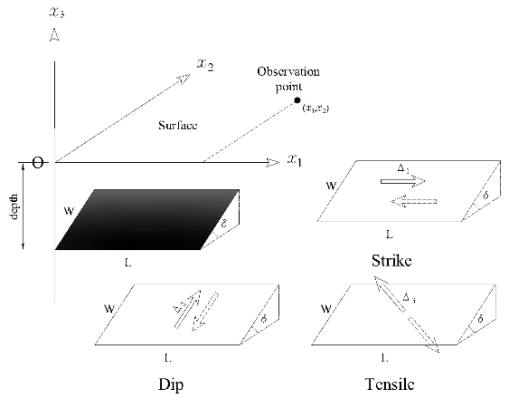

Fig. 1: Geometry of fault

Consider a rectangular fault with length, *L*, along the fault strike direction, and width, *W*, along a perpendicular direction to the strike in an FGTI half-space as shown in Fig. 1. The plane x_1–x_2 is the free surface of the half-space and $x_3 \leq 0$ is the problem domain. The axis of symmetry of the FGTI material is assumed to be parallel to the x_3-axis. Δ_1, Δ_2, and Δ_3 are strike-slip, dip-slip, and tensile components of the dislocation, respectively. The strike direction and the dip angle of the fault are represented by ϕ and δ, respectively.

2.1 Displacement discontinuity

The elastic deformation due to shear and tensile polygonal fault in a TI half-space was solved by [12]. Therefore, by using these solutions, the displacement induced by a strike-slip, dip-slip, and tensile fault in a TI half-space is expressed as:

For strike-slip fault,

$$u_i = -\Delta_1 \{\cos\phi U_{i1} + \sin\phi U_{i2}\} \tag{1}$$

For dip-slip fault,

$$u_i = \Delta_2 \{\sin\phi\cos\delta U_{i1} - \cos\phi\cos\delta U_{i2} - \sin\delta U_{i3}\} \tag{2}$$

For tensile fault,

$$u_i = -\Delta_3 \{\sin\phi\sin\delta U_{i1} - \cos\phi\sin\delta U_{i2} + \cos\delta U_{i3}\} \tag{3}$$

where

$$U_{ij} = U_{ij}^{\infty} + U_{ij}^{c} \tag{4}$$

and U_{ij} is the i^{th}-component of displacement for a unit given dislocation in the *j*-direction and superscript infinity and *c* denote the full-space and complementary part of the response.

2.2 Stress discontinuity

Based on recent studies by Kalantari and others [28-30, 32, 40], the displacement field in stress discontinuity is expressed by solving Fredholm dual integral equation as below:

$$\begin{aligned}
&\zeta_A(r) + \frac{l_2}{l_1}\left[\int_r^a \frac{\zeta_B(\rho)}{\rho} d\rho - \zeta_B(r)\right] \\
&+ \int_0^a K_{AA}(r,\rho)\zeta_A(\rho)d\rho + \int_0^a K_{AB}(r,\rho)\zeta_A(\rho)d\rho = \delta \\
&\zeta_B(r) + \frac{l_2}{l_1}\left[\frac{1}{r}\int_0^r \zeta_A(\rho)d\rho - \zeta_A(r)\right] \\
&+ \int_0^a K_{BB}(r,\rho)\zeta_A(\rho)d\rho + \int_0^a K_{BA}(r,\rho)\zeta_A(\rho)d\rho = 0
\end{aligned} \tag{5}$$

where

$$\begin{aligned}
&K_{AA}(r,\rho) = \sqrt{r\rho}\int_0^{\infty} \xi H_2(\xi) J_{-\frac{1}{2}}(r\xi) J_{-\frac{1}{2}}(\rho\xi) d\xi \\
&K_{BB}(r,\rho) = \sqrt{r\rho}\int_0^{\infty} \xi H_1(\xi) J_{\frac{3}{2}}(r\xi) J_{\frac{3}{2}}(\rho\xi) d\xi \\
&K_{AB}(r,\rho) = K_{BA}(\rho,r) = \\
&-\frac{l_2}{l_1}\sqrt{r\rho}\int_0^{\infty} \xi H_2(\xi) J_{-\frac{1}{2}}(r\xi) J_{\frac{3}{2}}(\rho\xi) d\xi
\end{aligned} \tag{6}$$

Other parameters can be found in [27-30, 32, 40].

To the best of the authors` knowledge, there is no closed-form solution for equations (5) and (6) in general form ("A key characteristic of these kinds of equations is that they have mathematical properties which make it difficult to obtain useful solutions by straightforward methods" [33]). Also, due to the oscillatory nature of Bessel functions in kernels of integral equations, the trapezoidal and Simpson rules are not efficient in which equal intervals are used. Considering the above reasons, the adaptive quadrature method is appropriate for numerical evaluation. Based on [14] the relations between solutions of the displacement discontinuity and stress discontinuity are the representation of Betti's reciprocal theorem, in which, if one has the stress discontinuity solution, the corresponding displacement

discontinuity can be found. Accordingly, by combining the result of section 2.1 and the solution of section 2.2, the solution of finite fault dislocation in the FGTI medium can be extracted.

2.3 Material properties

The elastic stiffness tensor C_{ijkl} for a TI material, when the plane of isotropy is parallel to the surface of half-space, is expressed as:

$$\begin{aligned} C_{ijkl} &= (C_{11}-2C_{66})\delta_{ij}\delta_{kl}+C_{66}\left(\delta_{ik}\delta_{jl}+\delta_{il}\delta_{jk}\right) \\ &+(C_{11}+C_{33}-2C_{13}-4C_{44})\delta_{i3}\delta_{j3}\delta_{k3}\delta_{l3} \\ &+(C_{13}-C_{11}+2C_{66})\left(\delta_{i3}\delta_{j3}\delta_{kl}+\delta_{k3}\delta_{l3}\delta_{ij}\right) \\ &+(C_{44}-C_{66})\left(\delta_{j3}\delta_{k3}\delta_{il}+\delta_{i3}\delta_{l3}\delta_{jk}+\delta_{j3}\delta_{l3}\delta_{ik}+\delta_{i3}\delta_{k3}\delta_{jl}\right) \end{aligned} \tag{7}$$

where δ_{ij} is the Kronecker delta, and C_{ij} is the elastic constant. In the FGTI medium, the elastic constants are assumed to vary in the z-direction as [25, 28-30, 34, 35, 40]:

$$C_{ij}(z)=C_{ij}e^{2\beta z} \tag{8}$$

where β indicates the exponential factor characterizing the degree of the material gradient in the z-direction constants. The material constants for an isotropic medium are also written as:

$$C_{11}=C_{33}=\lambda+2\mu,\ C_{12}=C_{13}=\lambda,\ C_{44}=C_{66}=\mu \tag{9}$$

where λ and μ are Lame's constants.

3. Verification and Numerical Examples

Before applying our solutions to a general fault dislocation embedded in a TI or FGTI half-space, the first numerical example (number 1) in observation point (25, 15) km is compared with the [8] problem which is related to a rectangular fault in an isotropic half-space.

Consider a rectangular fault with a length of 12 km and width of 8 km in which the lower edge is located at 10 km below the free surface and the azimuth and the dip angle of the fault are equal to zero and 40°, respectively. In addition, the medium is considered isotropic by a low, middle, and top range of Poisson's ratio. The displacements for different fault modes are also shown by dimensionless parameters u_{ij}/Δ_j which i denotes displacement in x_i direction due to j type of faults (j=1,2,3; 1: strike; 2: dip; 3: tensile).

In the following examples, the effects of the medium anisotropy on displacements are investigated. As mentioned previously, the soils are inherently anisotropic media and the source of anisotropy may be intrinsic (due to deposition, overburden, and confining pressure) or extrinsic (formed by stress-induced cracking of intrinsically isotropic rocks). In this article, Beryl rock and Mat I as real TI materials are selected [36-37]. For comparison, the corresponding Voigt average (VA) is also used to calculate the induced response in the equivalent isotropic half-space (Table. 1). The VA assumes $C_{ijij}^{aniso}=C_{ijij}^{iso}$ and $C_{iijj}^{aniso}=C_{iijj}^{iso}$, and hence for TI materials, the VA is defined as:

$$\begin{aligned} \hat{\lambda} &\cong \frac{C_{11}+C_{33}+5C_{12}+8C_{13}-4C_{44}}{15} \\ \hat{\mu} &\cong \frac{7C_{11}-5C_{12}+2C_{33}+12C_{44}-4C_{13}}{30} \end{aligned} \tag{10}$$

in which $\hat{\lambda}$ and $\hat{\mu}$ are the equivalent Lame constants.

Table 1: Material properties and the equivalent Lame constants

	Beryl rock	Mat I	$\hat{\lambda}$	$\hat{\mu}$
C_{11}	41.3	113	Beryl rock	
C_{33}	36.2	87	12.79	12.25
C_{44}	10	30	Mat I	
C_{66}	13.3	41.5	27.07	36.23
C_{13}	10.1	22		

3.1 Isotropic materials

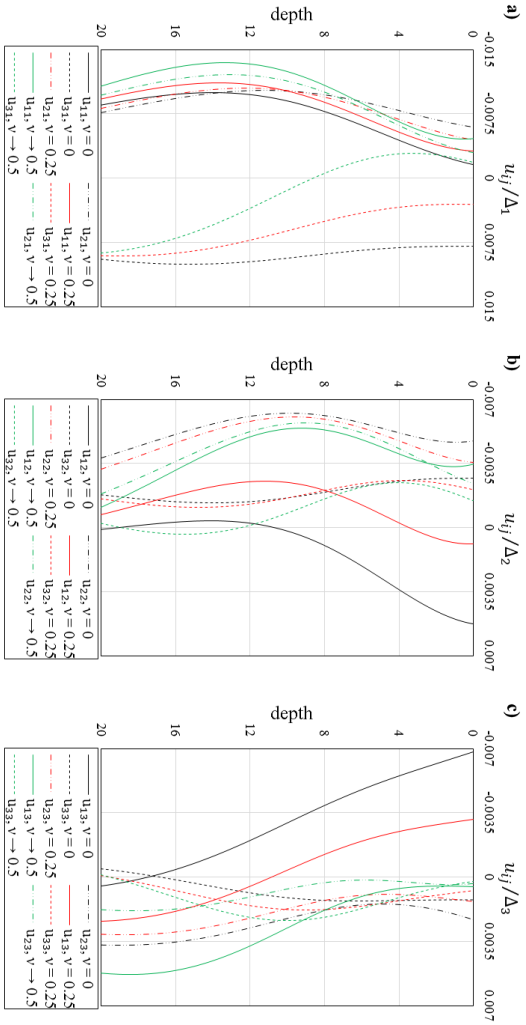

Fig. 2: Displacement along the depth (km) for a) Strike-slip, b) Dip-slip, and c) Tensile fault

Figure 2 shows displacement at the observation point (25, 15) in x_i direction along the depth for various Poisson's ratios in different fault modes (strike, dip, and tensile fault). Comparing with available literature shows that the results

are the same as the results in [8] for $\nu = 0.25$. Also, based upon the introduced dimensionless parameters (u_{ij}/Δ_j), exact displacements can be easily found by changing the dislocation amplitude (Δ_j).

The agreement of the results in the isotropic case confirms the accuracy, efficiency, and reliability of the proposed procedure to evaluate the effect of non-homogeneity on the dislocation problem.

3.2 Transversely isotropic materials (Beryl rock)

Figures. 3 and 4 show the responses of another example (number 2) for a rectangular fault with a length of 39 km and width of 16 km which the lower edge is located at 18 km below the free surface and the dip angle of the fault is 17°.

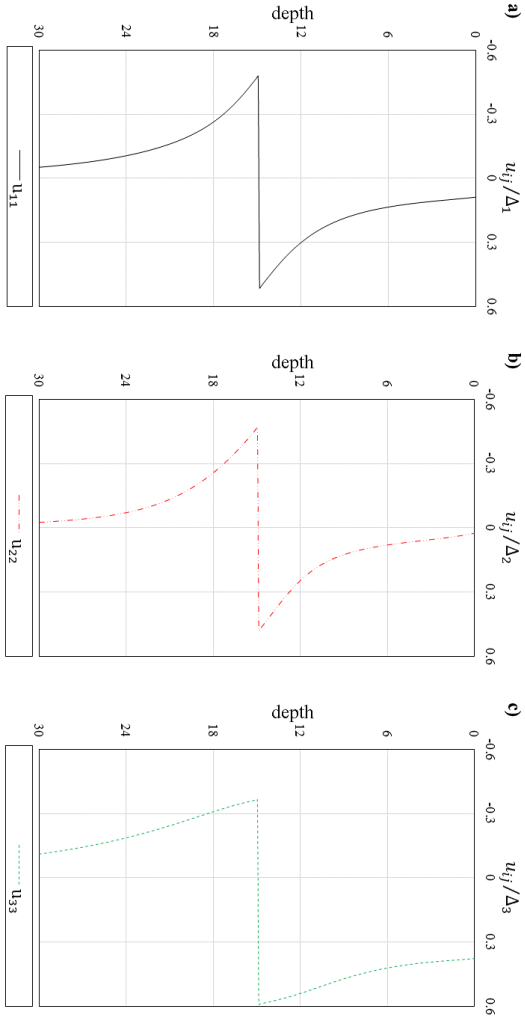

Fig. 3. Displacement along the depth (km) for a) Strike-slip, b) Dip-slip, and c) Tensile fault in (5,10) km

The medium is considered TI as Table. 1 and displacements for different fault modes are shown by dimensionless parameters u_{ij}/Δ_j in two observation points (5, 10) km and (-5, -10) km, in which the first observation point is in the fault image on the free surface (Figure 3) and the second one is out of the area (Figure 4).

Figure 3 shows displacement along the depth for different dislocation modes when the observation point is in the fault image on the free surface. In this figure, discontinuity in displacement near the fault area shows that the boundary conditions perfectly match assumptions.

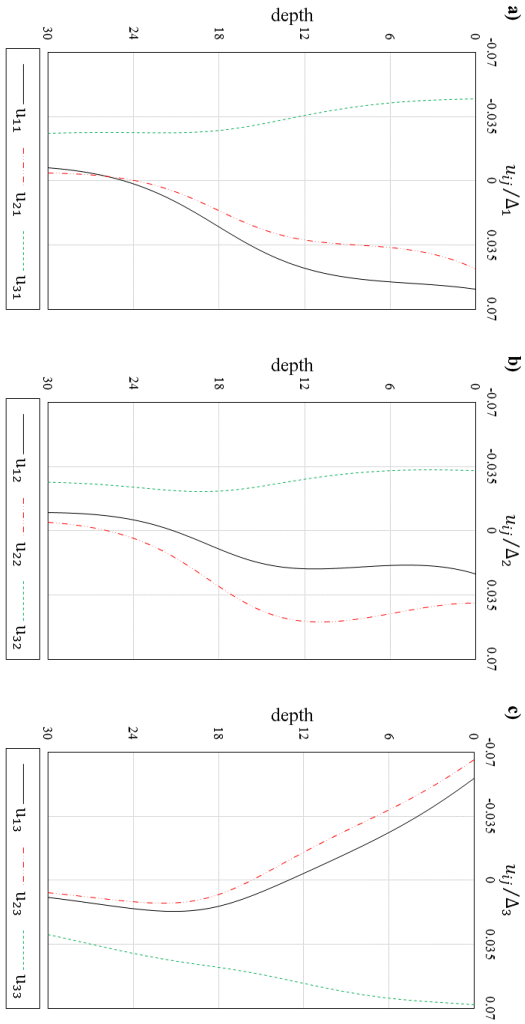

Fig. 4: Displacement along the depth (km) for a) Strike-slip, b) Dip-slip, and c) Tensile fault in (-5, -10) km

3.3 Functionally graded transversely isotropic materials (Beryl rock)

Figure 5 shows the results of another example (number 3) for a horizontal square fault with a length of 10 km which the lower edge is located at 15 km below the free surface. To show the impact of materials properties on surface displacements, TI materials and their equivalent isotropic material (VA) are considered (Table. 1). In addition, the Figure shows the impact of non-homogeneity on the responses by considering different β parameters.

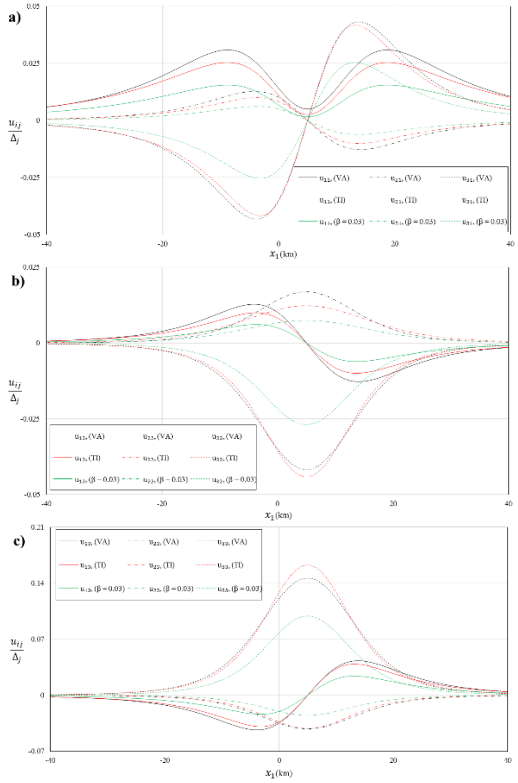

Fig. 5a. Surface displacement along the x_1 direction for a) Strike-slip, b) Dip-slip, and c) Tensile fault

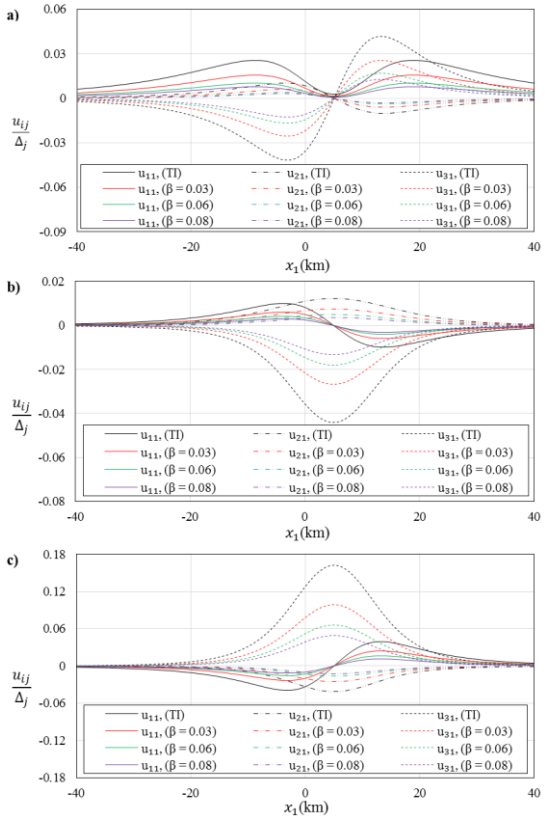

Fig. 5b. Surface displacement along the x_1 direction for a) Strike-slip, b) Dip-slip, and c) Tensile fault

It is observed from Figure 5 that there is a major difference between FGTI, TI, and VA. The results show that simplifying assumptions as isotropic media causes poor approximation for considering soil and the simplified results are not reliable. Also, as indicated in Figure 5, the larger the degree of β parameter, the smaller the displacement results. Since the larger the value of β, the larger the wave velocity results in, which means the stiffer soils and causes less displacement.

3.4 Subtraction of transversely isotropic materials and Voigt average (Mat I)

Figures. 6-8 shows the displacements in a rectangular fault in Mat I, with a length of 20 km and width of 10 km which the lower edge is located at 15 km below the free surface, and the dip angle of the fault is 45° (example number 4).

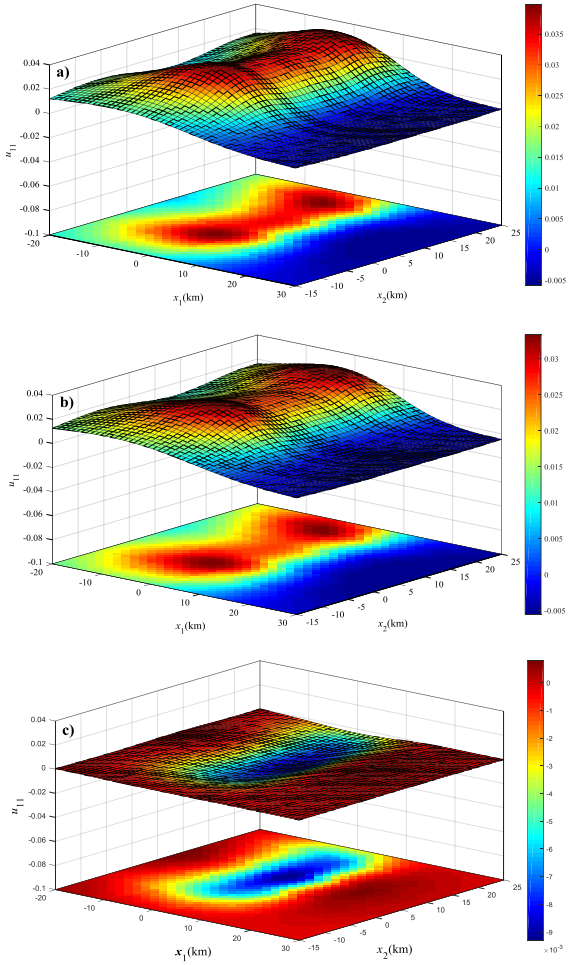

Fig. 6. Surface displacement for strike-slip fault in strike direction for a) VA, b) TI, and c) Subtraction of (a) and (b)

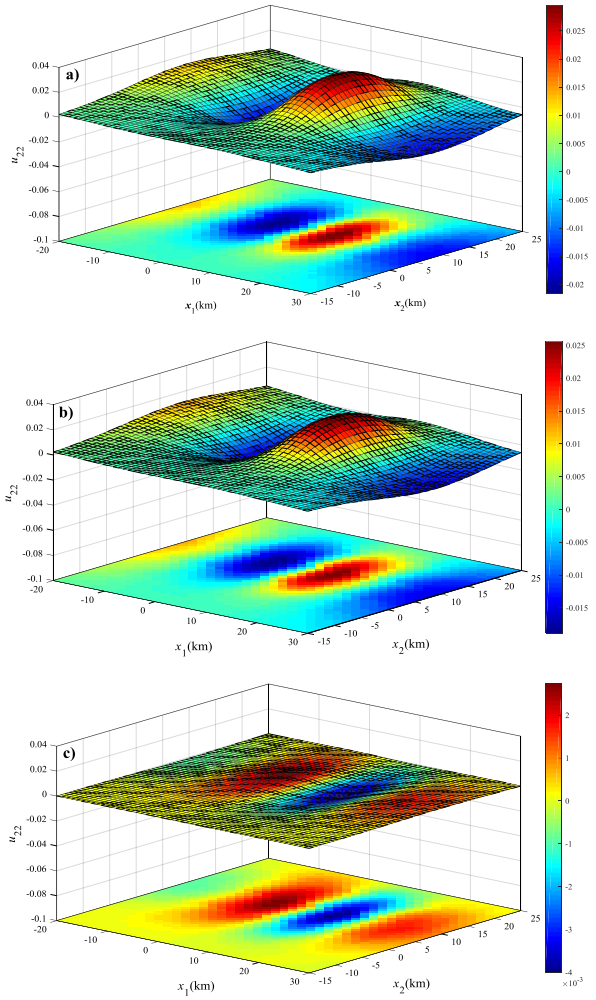

Fig.7. Surface displacement for dip-slip fault in dip direction for a) VA, b) TI, and c) Subtraction of (a) and (b)

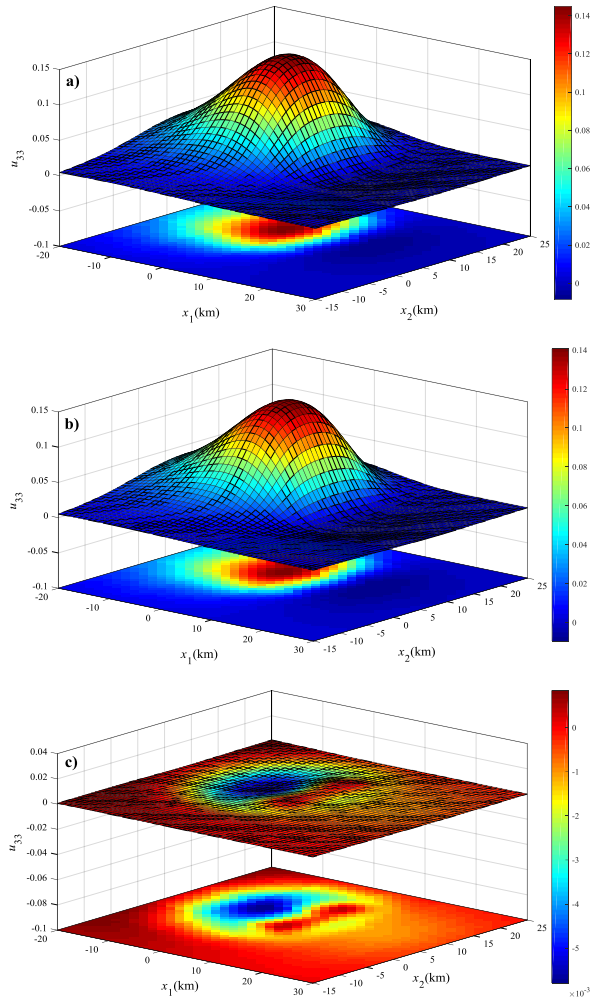

Fig.8. Surface displacement for tensile fault in the fault normal direction for a) VA, b) TI, and c) Subtraction of (a) and (b)

Figures 7 and 8 clearly show the difference between the TI and VA is significant. Thus, the non-homogeneity of the medium should be considered to accurately predict the response in TI or TIFG medium.

4. Simple Slip Inversion

There are many scientific reasons why detailed knowledge of the earthquake source is valuable, and the destructive effects of earthquakes are a motivation to learn as much as possible about their nature and effects. Since direct measurement of the source activity is not feasible, one can learn about the source only from distant (weak motion) and near (strong motion) records. The inversion can be associated with different source parameters, depending on the mathematical model, but ultimately the goal is to learn as much as possible about the nature of the source. In earthquake engineering, understanding the earthquake source is important for ground motion prediction from possible future earthquakes, which is needed for the seismic design of structures.

The characterization of the earthquake source from recorded data is an inverse type of problem, i.e., one in which the input of a system has to be determined from the output.

4.1 Data and model parameter

The final goal of scientists and engineers is to find a relation between physical parameters as models to some set of data as responses. This relation in many physical phenomena can be introduced by Green's functions that play system functions to describe the relations between models and data sets. Thus, generating an exact and appropriate system function that introduces the medium properties in a good way is a priority. Based on our previous studies [28-30, 32, 40], extracted Green's function can be used in a forward problem. In this part, a simple way to solve an inverse problem is suggested.

Consider function G which describes the relationship between the model (m) and data (d):

$$\mathrm{G}(m)=d \tag{11}$$

In practice, d may be a function of time, space, or a collection of discrete observations. An important issue is

that actual observations always contain some amount of noise. Two common ways that noise may arise are calibration influences on instruments and numerical round-off. Thus, the data can be considered as generally consisting of noiseless observations from a "perfect" experiment, d_{true}, plus a noise component η:

$$d = \mathrm{G}(m_{\text{true}}) + \eta \Rightarrow d_{\text{true}} + \eta \tag{12}$$

where d_{true} satisfies equation (11) for m equal to the true model (m_{true}). Although it is mathematically possible to separate noise from data, it is impossible in practical applications due to the mentioned reasons. This problem (divide noise from data) is left to seismologists; however, the point is to know that a random error can be added to the data set for simulation of a real condition.

4.2 Fault Geometry, soil properties, and preparing inverse model

We assumed that the fault dimensions and depth are found by using GBIS software as used by [38] or using a grid search on fault geometry. Also, the TI elasticity constants (soil properties) can be found by the single-plug or three-plug method as used by [39]. By considering mentioned description, we have all the basic information to build a discrete linear inverse problem (G by having soil properties and data on the surface by measuring displacements).

$$\begin{bmatrix} \begin{Bmatrix} u_{11}^{n_1} & u_{12}^{n_1} & u_{13}^{n_1} \\ u_{21}^{n_1} & u_{22}^{n_1} & u_{23}^{n_1} \\ u_{31}^{n_1} & u_{32}^{n_1} & u_{33}^{n_1} \end{Bmatrix} \\ \mathrm{M} \\ \begin{Bmatrix} u_{11}^{n_k} & u_{12}^{n_k} & u_{13}^{n_k} \\ u_{21}^{n_k} & u_{22}^{n_k} & u_{23}^{n_k} \\ u_{31}^{n_k} & u_{32}^{n_k} & u_{33}^{n_k} \end{Bmatrix} \end{bmatrix} \begin{Bmatrix} \begin{Bmatrix} \Delta_1^1 \\ \Delta_2^1 \\ \Delta_3^1 \end{Bmatrix} \\ \mathrm{M} \\ \begin{Bmatrix} \Delta_1^n \\ \Delta_2^n \\ \Delta_3^n \end{Bmatrix} \end{Bmatrix} = \begin{Bmatrix} \begin{Bmatrix} u_1^{n_1} \\ u_2^{n_1} \\ u_3^{n_1} \end{Bmatrix} \\ \mathrm{M} \\ \begin{Bmatrix} u_1^{n_k} \\ u_2^{n_k} \\ u_3^{n_k} \end{Bmatrix} \end{Bmatrix} \tag{13}$$

by using equations (1), (2) and (12), we can write a linear system of algebraic equations as above, where superscript n_k indicates k^{th} observation point on a free surface.

As is clear from equation (13), when the number of observation points are selected more than one point, the matrix G is not square and cannot be determined in common ways. So, we can fix the problem by using SVD (singular value decomposition) to achieve model parameters.

5. Conclusions

Based on the concepts of displacement dislocation and stress dislocation (stress jump), the general rectangular fault in a three-dimensional FGTI half-space was considered.

The applicability and robustness of the presented solution are demonstrated by some numerical examples as a special case and the results show complete agreement with the literature.

The numerical examples revealed the important effect of material anisotropy on internal and surface deformations. Furthermore, the numerical results show a significant difference in displacement, which emphasizes why considering a realistic material for a real ground motion simulation is imperative. Also, as indicated in the figures, the larger the degree of β parameter, the smaller the displacement results in.

In addition, a simple formulation by using data on a surface is proposed for extracting the dislocations vector in the fault plane.

References

[1] Lamb, H. (1904). I. On the propagation of tremors over the surface of an elastic solid. *Philosophical Transactions of the Royal Society of London. Series A, Containing papers of a mathematical or physical character*, *203*(359-371), 1-42.

[2] Steketee, J. A. (1958). On Volterra's dislocations in a semi-infinite elastic medium. *Canadian Journal of Physics*, *36*(2), 192-205.

[3] Maruyama, T. (1964). 16. Statical elastic dislocations in an infinite and semi-infinite medium. *Bull. Earthq. Res. Inst*, *42*, 289-368.

[4] Robertson, I. A. (1966). Forced vertical vibration of a rigid circular disc on a semi-infinite elastic solid. In *Mathematical proceedings of the Cambridge philosophical society* (Vol. 62, No. 3, pp. 547-553). Cambridge University Press.

[5] Apsel, R. J., & Luco, J. E. (1976). Torsional response of rigid embedded foundation. *Journal of the Engineering Mechanics Division*, *102*(6), 957-970.

[6] Higashihara, H. (1984). Explicit Green's function approach to forced vertical vibrations of circular disk on semi-infinite elastic space. *Journal of engineering mechanics*, *110*(10), 1510-1523.

[7] Okada, Y. (1985). Surface deformation due to shear and tensile faults in a half-space. *Bulletin of the seismological society of America*, *75*(4), 1135-1154.

[8] Okada, Y. (1992). Internal deformation due to shear and tensile faults in a half-space. *Bulletin of the seismological society of America*, *82*(2), 1018-1040.

[9] Thongchom, C., Roodgar Saffari, P., Roudgar Saffari, P., Refahati, N., Sirimontree, S., Keawsawasvong, S., & Titotto, S. (2022b). Dynamic response of fluid-conveying hybrid smart carbon nanotubes considering slip boundary conditions under a moving nanoparticle. *Mechanics of Advanced Materials and Structures*, 1-14.

[10] Moshtagh, E., Eskandari-Ghadi, M., & Pan, E. (2019). Time-harmonic dislocations in a multilayered transversely isotropic magneto-electro-elastic half-space. *Journal of Intelligent Material Systems and Structures*, *30*(13), 1932-1950.

[11] Wang, C. D., Tzeng, C. S., Pan, E., & Liao, J. J. (2003). Displacements and stresses due to a vertical point load in an inhomogeneous transversely isotropic half-space. *International Journal of Rock Mechanics and Mining Sciences*, *40*(5), 667-685.

[12] Pan, E., Yuan, J. H., Chen, W. Q., & Griffith, W. A. (2014). Elastic deformation due to polygonal dislocations in a transversely

isotropic half-space. *Bulletin of the Seismological Society of America*, *104*(6), 2698-2716.

[13] Molavi Tabrizi, A., & Pan, E. (2015). Time-dependent displacement and stress fields due to shear and tensile faults in a transversely isotropic viscoelastic half-space. *Geophysical Journal International*, *202*(1), 163-174.

[14] Pan, E., & Chen, W. (2015). *Static green's functions in anisotropic media*. Cambridge University Press.

[15] Pan, E., Molavi Tabrizi, A., Sangghaleh, A., & Griffith, W. A. (2015). Displacement and stress fields due to finite faults and opening-mode fractures in an anisotropic elastic half-space. *Geophysical Journal International*, *203*(2), 1193-1206.

[16] Pan, E., Griffith, W. A., & Liu, H. (2019). Effects of generally anisotropic crustal rocks on fault-induced displacement and strain fields. *Geodesy and Geodynamics*, *10*(5), 394-401.

[17] Han, Z., Lin, G., & Li, J. (2015). Dynamic impedance functions for arbitrary-shaped rigid foundation embedded in anisotropic multilayered soil. *Journal of Engineering Mechanics*, *141*(11), 04015045.

[18] Singh, A. K., Koley, S., Negi, A., & Ray, A. (2019). On the dynamic behavior of a functionally graded viscoelastic-piezoelectric composite substrate subjected to a moving line load. *The European Physical Journal Plus*, *134*(3), 1-22.

[19] Attia, M. A., & El-Shafei, A. G. (2020). Investigation of multibody receding frictional indentation problems of unbonded elastic functionally graded layers. *International Journal of Mechanical Sciences*, *184*, 105838.

[20] Azaripour, S., & Baghani, M. (2019). Vibration analysis of FG annular sector in moderately thick plates with two piezoelectric layers. *Applied Mathematics and Mechanics*, *40*(6), 783-804.

[21] Yas, M. H., & Moloudi, N. (2015). Three-dimensional free vibration analysis of multi-directional functionally graded piezoelectric annular plates on elastic foundations via state space based differential quadrature method. *Applied Mathematics and Mechanics*, *36*(4), 439-464.

[22] Martin, P. A., Richardson, J. D., Gray, L. J., & Berger, J. R. (2002). On Green's function for a three–dimensional exponentially graded elastic solid. *Proceedings of the Royal Society of London. Series A: Mathematical, Physical and Engineering Sciences*, *458*(2024), 1931-1947.

[23] Roshanbakhsh, M. Z., Tavakkoli, S. M., & Neya, B. N. (2020). Free vibration of functionally graded thick circular plates: An exact and three-dimensional solution. *International Journal of Mechanical Sciences*, *188*, 105967.

[24] Thongchom, C., Jearsiripongkul, T., Refahati, N., Roudgar Saffari, P., Roodgar Saffari, P., Sirimontree, S., & Keawsawasvong, S. (2022a). Sound transmission loss of a honeycomb sandwich cylindrical shell with functionally graded porous layers. *Buildings*, *12*(2), 151.

[25] Çömez, İ. (2015). Contact problem for a functionally graded layer indented by a moving punch. *International Journal of Mechanical Sciences*, *100*, 339-344.

[26] Eskandari, M., & Shodja, H. M. (2010). Green's functions of an exponentially graded transversely isotropic half-space. *International Journal of Solids and Structures*, *47*(11-12), 1537-1545.

[27] Eskandari-Ghadi, M., & Amiri-Hezaveh, A. (2014). Wave propagations in exponentially graded transversely isotropic half-space with potential function method. *Mechanics of Materials*, *68*, 275-292.

[28] Kalantari, M., Khaji, N., & Eskandari-Ghadi, M. (2021). Rocking forced displacement of a rigid disc embedded in a functionally graded transversely isotropic half-space. *Mathematics and Mechanics of Solids*, *26*(7), 1029-1052.

[29] Kalantari, M., & Khaji, N. (2022). Torsion vibration of foundation in a functionally graded transversely isotropic, linearly elastic half-space. *Forces in Mechanics*, 100082.

[30] Kalantari, M., Khaji, N., Eskandari-Ghadi, M., & Keawsawasvong, S. (2022). Dynamic Analysis of a Vertically Loaded Rigid Disc in a Functionally Graded Transversely Isotropic Half-Space. *Transportation Infrastructure Geotechnology*, 1-25.

[31] Yuan, J. H., Pan, E., & Chen, W. Q. (2013). Line-integral representations for the elastic displacements, stresses and interaction energy of arbitrary dislocation loops in transversely isotropic bimaterials. *International Journal of Solids and Structures*, *50*(20-21), 3472-3489.

[32] Kalantari, M., Khojasteh, A., Mohammadnezhad, H., Rahimian, M., & Pak, R. Y. S. (2015). An inextensible membrane at the interface of a transversely isotropic bi-material full-space. *International Journal of Engineering Science*, *91*, 34-48.

[33] Aster, R. C., Borchers, B., & Thurber, C. H. (2018). *Parameter estimation and inverse problems*. Elsevier.

[34] Shahmohamadi, M., Khojasteh, A., Rahimian, M., & Pak, R. (2017). The frictionless axial interaction of a rigid disk with a two-layered functionally graded transversely isotropic medium. *Mathematics and Mechanics of Solids*, *22*(6), 1407-1424.

[35] Nirwal, S., Sahu, S. A., Baroi, J., & Saroj, P. K. (2021). Analysis of wave scattering in 3-layer piezo composite structure [Pb [Zr x Ti1-x] O3-ALN-Pb [Zr x Ti1-x] O3]. *Mechanics Based Design of Structures and Machines*, *49*(3), 307-328.

[36] Ding, H., Chen, W., & Zhang, L. (2006). *Elasticity of transversely isotropic materials* (Vol. 126). Springer Science & Business Media.

[37] Godfrey, N. J., Christensen, N. I., & Okaya, D. A. (2000). Anisotropy of schists: Contribution of crustal anisotropy to active source seismic experiments and shear wave splitting observations. *Journal of Geophysical Research: Solid Earth*, *105*(B12), 27991-28007.

[38] Vajedian, S., Motagh, M., Mousavi, Z., Motaghi, K., Fielding, E., Akbari, B., ... & Darabi, A. (2018). Coseismic deformation field of the Mw 7.3 12 November 2017 Sarpol-e Zahab (Iran) earthquake: A decoupling horizon in the northern Zagros Mountains inferred from InSAR observations. *Remote Sensing*, *10*(10), 1589.

[39] Wang, Z. (2002). Seismic anisotropy in sedimentary rocks, part 1: A single-plug laboratory method. *Geophysics*, *67*(5), 1415-1422.

[40] Kalantari, M., & Khaji, N. (2022). Response of rigid circular plate in a functionally graded transversely isotropic, half-space under horizontal steady-state excitation. *Mechanics Based Design of Structures and Machines*, 1-24 (in press).

This article is an open-access article distributed under the terms and conditions of the Creative Commons Attribution (CC-BY) license.